Inorganic Chemistry

Article

pubs.acs.org/IC

Bilayer Mott System Based on Ni(dmit)$_2$ (dmit = 1,3-dithiole-2-thione-4,5-dithiolate) Anion Radicals: Two Isostructural Salts Exhibit Contrasting Magnetic Behavior

Tetsuro Kusamoto,* Hiroshi M. Yamamoto,[†,‡] Naoya Tajima,[§] Yugo Oshima, Satoshi Yamashita,[∥] and Reizo Kato

RIKEN, Wako, Saitama 351-0198, Japan

Supporting Information

ABSTRACT: A new class of Ni(dmit)$_2$ anion radical salt (Et-2,5-DBrP)[Ni(dmit)$_2$]$_2$ (**1**) (Et-2,5-DBrP = ethyl-2,5-dibromopyridinium) was developed. Single-crystal X-ray diffraction analysis indicates that this salt contains two crystallographically independent anion layers in the crystal with effective Br···S halogen bonds between the cation and the anion. The crystal and electronic structures, and electrical and magnetic measurements reveal that **1** is a novel *bilayer Mott system*, in which two different Mott-insulating anion layers coexist in one crystal. Selective halogen substitution of Br with I at the 2-position in the cation affords the isostructural bilayer salt (Et-2I-5BrP)[Ni(dmit)$_2$]$_2$ (**2**) (Et-2I-5BrP = ethyl-2-iodo-5-bromopyridinium), while substitution at the 5-position results in a structural change, yielding the monolayer salt (Et-2Br-5IP)[Ni(dmit)$_2$]$_2$ (**3**) (Et-2Br-5IP = ethyl-2-bromo-5-iodopyridinium). These results indicate that the halogen bond plays an important role to realize the bilayer system, and that the crystal structure is controlled by tuning the strength of the halogen bond. The low temperature magnetic properties of the two isostructural salts **1** and **2** are significantly different, because they are affected by fluctuated spins that do not participate in the formation of short-range antiferromagnetic domains. The bilayer salt generates the fluctuated spins more easily than conventional monolayer salts, and such fluctuated spins are expected to result in unique physical properties.

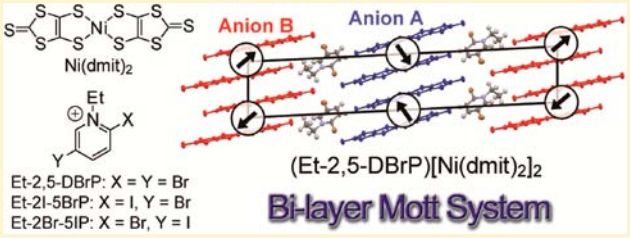

INTRODUCTION

Metal dithiolene complexes form an important class of functional materials that exhibit exotic conducting and magnetic properties.[1,2] Among these complexes, M(dmit)$_2$ (dmit = 1,3-dithiole-2-thione-4,5-dithiolate; M = Ni, Pd, Pt, Au) anion radicals have provided a wide variety of molecular conductors including metallic conductors and superconductors.[2] M(dmit)$_2$ has 10 peripheral S atoms, which enables a multidimensional electrical network via intermolecular S···S contacts in the solid state. An interesting electronic character of M(dmit)$_2$ is that the electron density is well distributed onto the S atoms in the highest occupied molecular orbitals (HOMO) and the lowest unoccupied molecular orbital (LUMO), and the HOMO−LUMO energy gap Δ is small (<1 eV).[3] The HOMO has a_{2u} symmetry while the LUMO has b_{2g} symmetry. The metal d_{xz} orbital mixes into the LUMO, while the HOMO has no contribution from the metal d orbitals because of the symmetry. The electronic and molecular structures of the M(dmit)$_2$ anion radical are dependent on the central metal ion. Pd(dmit)$_2$ anion radicals tend to dimerize strongly through Pd−Pd bond formation in the solid state. This dimerization and small Δ induce a HOMO−LUMO band inversion in the electronic structure.[3] In a system with a narrow and half-filled energy band, where each unit in the crystal has one conduction electron, strong on-site Coulomb repulsion is known to induce an electrically insulating state (Mott insulating state).[4] Most β'-type Pd(dmit)$_2$ anion radical salts exhibit a Mott insulating state, and perform diverse electronic (magnetic) ground states including antiferromagnetic long-range ordering,[5] charge separation,[6] valence-bond solid,[7] and quantum spin liquid.[8] The electrons in these salts are localized at each [Pd(dmit)$_2$]$_2^-$ unit to avoid on-site Coulomb repulsion, and the spin degree of freedom plays a crucial role in determining the physical properties. Meanwhile, Ni(dmit)$_2$ anion radicals have less tendency to form dimer units, which permits a diversity of molecular arrangements, orientations, and oxidation states in the crystal.[9]

Most Ni(dmit)$_2$ anion radical salts contain one kind of crystallographically independent anion layer in the crystal lattice, i.e., a *monolayer system*, as observed in the Ni(dmit)$_2$-based superconductor (Me$_4$N)[Ni(dmit)$_2$]$_2$.[10] On the other hand, we have disclosed that the introduction of supramolecular cation···anion interaction into the Ni(dmit)$_2$ molecular system can provide a novel molecular packing mode, a so-called *bilayer system*, which contains two crystallographically independent (nonequivalent) anion layers in one crystal lattice. (Me$_3$Te)[Ni(dmit)$_2$]$_2$ is a representative bilayer

Received: July 16, 2012
Published: October 5, 2012

   dx.doi.org/10.1021/ic301552z | *Inorg. Chem.* 2012, 51, 11645−11654

$Ni(dmit)_2$ anion radical salt that contains two crystallographically independent $Ni(dmit)_2$ anion layers (layers **A** and **B**) in the unit cell.[11] These two layers differ from each other in the anion arrangement. Three short Te···S contacts (secondary bonds) between the cations and the anions are evident in this salt; one between the cations and layer **A**, and the other two between the cations and layer **B**. Such sterically anisotropic Te···S contacts around the Me_3Te cation lowers the crystal symmetry, thereby yielding two different kinds of anion layers. This salt exhibits metallic conduction down to 60−70 K. It should be noted that the two different anion layers in this salt construct different conduction bands. Each band in the bilayer system can generally exhibit different dispersion, filling, Fermi surface, and physical properties. For example, the novel bilayer salt (Me-3,5-DIP)$[Ni(dmit)_2]_2$ (Me-3,5-DIP = methyl-3,5-diiodopyridinium, Chart 1) presents a unique electronic

Chart 1

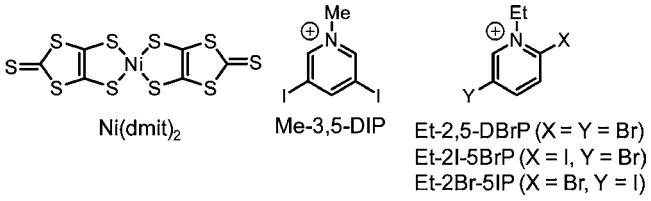

structure[12] with two crystallographically independent $Ni(dmit)_2$ anion layers (Layers **A** and **B**) that have different anion arrangements. The most interesting electronic feature of this salt is that layer **A** plays the role of a two-dimensional metallic conductor, whereas layer **B** is in a Mott insulating state and exhibits paramagnetism due to the localized spin on $[Ni(dmit)_2]_2^-$. This is an exotic example in which one kind of molecule, that is, the $Ni(dmit)_2$ anion radical, exhibits two contrasting properties in one crystal according to the particular arrangements. The electronic correlation between the conducting electrons in layer **A** and the magnetic spins in layer **B** was elucidated by ^{13}C nuclear magnetic resonance spectroscopy (NMR) and resistance and magnetic torque measurements.[12b,c] Interestingly, a significant negative magnetoresistance effect under 40 K is observed. In this salt, I···S halogen bonds between the Me-3,5-DIP cation and the $Ni(dmit)_2$ anion operate effectively. The halogen bond, defined as noncovalent intermolecular interactions involving halogens as electrophilic species, is strong and sufficiently directional to construct a supramolecular architecture in the molecular conductors.[13] As for the Me_3Te cation, the Me-3,5-DIP cation with low molecular symmetry induces an asymmetric steric environment around the cation to afford a bilayer structure.

Such bilayer salts can display novel electronic structures and physical properties, such as observed in (Me-3,5-DIP)$[Ni(dmit)_2]_2$, that are not obtained in the conventional monolayer salts. From this viewpoint, we intend to develop new bilayer salts based on $Ni(dmit)_2$ anion radicals and ethyl-2,5-dihalopyridinium cations. These cations have two halogen atoms and an asymmetric molecular structure; therefore, the effective halogen bond between the cation and anion together with the low molecular symmetry of the cation is expected to result in novel bilayer structures.

In this study, we prepared a new bilayer $Ni(dmit)_2$ anion radical salt (Et-2,5-DBrP)$[Ni(dmit)_2]_2$ (**1**). The Et-2,5-DBrP cation contains two Br atoms that are available as halogen bond donors (Chart 1). Single-crystal X-ray diffraction (XRD) analysis indicates that this salt contains two crystallographically independent anion layers in the crystal with effective Br···S halogen bonds between the cation and the anion. A band structure calculation based on the tight-binding approximation, in addition to electrical and magnetic measurements, revealed that this salt is a novel *bilayer Mott system* with two anion layers forming different types of Mott insulating states. Selective halogen substitution of Br with I at the 2-position in the cation afforded an isostructural bilayer salt (Et-2I-5BrP)$[Ni(dmit)_2]_2$ (**2**), while substitution at the 5-position caused a structural change and yielded the monolayer salt (Et-2Br-5IP)$[Ni(dmit)_2]_2$ (**3**). The low temperature magnetic properties of the two isostructural salts **1** and **2** were significantly different, which reflects the unique character of the bilayer system.

RESULTS AND DISCUSSION

Preparation of Cations and Halogen Bond Donor Ability of Et-2,5-DBrP. Ethyl-2,5-dihalopyridinium cations were prepared according to Scheme 1. 2,5-Dihalopyridines

Scheme 1

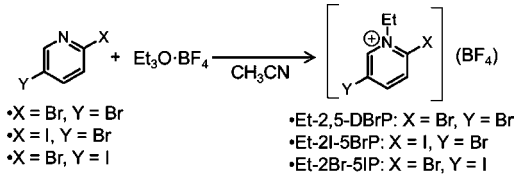

reacted with $Et_3O{\cdot}BF_4$ to yield the corresponding (Et-2,5-DBrP)BF_4, (Et-2I-5BrP)BF_4, and (Et-2Br-5IP)BF_4 salts. The halogen bond formation capability of the Br atoms in Et-2,5-DBrP was confirmed by analyzing the crystal structure of (Et-2,5-DBrP)$Br{\cdot}H_2O$, the single crystal of which was obtained by metathesis reaction between (Et-2,5-DBrP)BF_4 and $^nBu_4N{\cdot}Br$ in CH_3CN-Et_2O. Figure 1 shows that both crystallographically

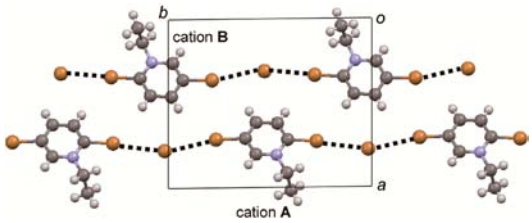

Figure 1. Crystal structure of (Et-2,5-DBrP)$Br{\cdot}H_2O$ viewed along the *c*-axis. Water molecules are omitted for clarity. Dotted lines represent halogen bonds between cation and anion.

independent Et-2,5-DBrP cations, **A** and **B**, form halogen bonds with Br^- anions. The $Br_{cation}\cdots Br_{anion}$ distances range from 3.244(2) to 3.427(2) Å, which are shorter than the sum of the van der Waals radii of two Br atoms (3.70 Å). The Br atoms in the cation of this crystal behave as Lewis acids (halogen bond donors), while the Br^- anion behaves as a Lewis base (halogen bond acceptor).[16] The positive charge on the cation is considered to assist the halogen bond donor ability. These results suggest the capability for halogen bond formation of the Br atoms in the cation.

Preparation of $Ni(dmit)_2$ Anion Radical Salts with Ethyl-2,5-dihalopyridinium Cations. Three $Ni(dmit)_2$ anion radical salts, (Et-2,5-DBrP)$[Ni(dmit)_2]_2$ (**1**), (Et-2I-

dx.doi.org/10.1021/ic301552z | Inorg. Chem. 2012, 51, 11645−11654

5BrP)[Ni(dmit)$_2$]$_2$ (**2**), and (Et-2Br-5IP)[Ni(dmit)$_2$]$_2$ (**3**), were obtained by galvanostatic electrolysis from a mixture of (^{n}Bu$_4$N)[Ni(dmit)$_2$] with a large excess of the corresponding (ethyl-2,5-dihalopyridinium)(BF$_4$) salt as the supporting electrolyte. Crystals of each salt that were suitable for single-crystal XRD analysis were grown on the anode.

Polymorphism was detected in the Et-2Br-5IP salt, where two (Et-2Br-5IP)[Ni(dmit)$_2$]$_2$ complexes (**3** and **4**) with similar appearance, but with different crystal structures, were obtained in the same batch. Several single crystal XRD measurements suggested that **3** is the main product. The XRD data quality for **4** was not sufficient; therefore, only the crystal structure of **3** is discussed here, and the crystal structure of **4** is reported in the Supporting Information.

Crystal and Electronic Structures of (Et-2,5-DBrP)[Ni(dmit)$_2$]$_2$ (1). The crystal structure of (Et-2,5-DBrP)[Ni(dmit)$_2$]$_2$ (**1**) is shown in Figure 2. The unit cell contains two

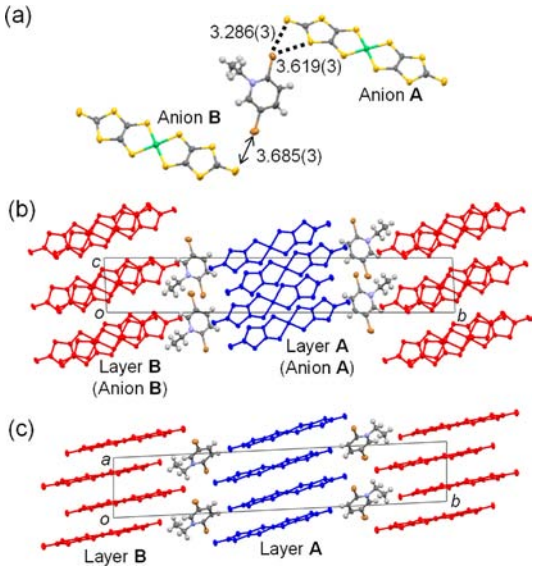

Figure 2. Crystal structure of (Et-2,5-DBrP)[Ni(dmit)$_2$]$_2$ (**1**): Crystallographically independent anions **A** and **B**, and cation. Halogen bonds and short atomic distance (Å) are depicted as dotted lines and arrow, respectively (a). Views along the ***a***-axis (b) and the ***c***-axis (c).

crystallographically independent Ni(dmit)$_2$ anions (**A** and **B**) and one crystallographically independent Et-2,5-DBrP cation. Each anion forms a planar molecular structure, in which the Ni atom adopts square-planar coordination geometry. Br···S halogen bonds are detected between the cation and the anion **A**, which are shorter than the sum of the van der Waals radii of S and Br atoms (3.65 Å), while a short Br···S distance (3.685(3) Å) is observed between the cation and the anion **B** (Figure 2a). This indicates that a low-symmetry steric environment is realized around the cation, which operates in favor of a bilayer structure. The average bond lengths in the anions **A** and **B** were compared with those in the [Ni(dmit)$_2$]$^-$ monoanion[14] and neutral Ni(dmit)$_2$[15] to estimate the formal oxidation states. The bond lengths in the Ni(dmit)$_2$ anion radical reflect the electron density distribution and phase of the LUMO (figure in Table 2), and are known to change according to the formal charge (oxidation state). As shown in Table 2, the bonds **a**, **b**, **f**, with antibonding nature are elongated upon reduction (from neutral Ni(dmit)$_2$ to [Ni(dmit)$_2$]$^-$ monoanion). Anions **A** and **B** have similar bond lengths, and the bond lengths of **a**, **b**, and **f** have intermediate values between those of [Ni(dmit)$_2$]$^-$ and [Ni(dmit)$_2$]^0. These results suggest that both anions **A** and **B** are in the same oxidation state, namely, [Ni(dmit)$_2$]$^{-0.5}$. The [Ni(dmit)$_2$]$^{-0.5}$ oxidation state of each anion is also supported by conductivity and magnetic measurements, as reported later.

The anions **A** and **B** are independently stacked to construct layered structures (layers **A** and **B**) parallel to the *ac* plane, as shown in Figures 2b and c. The anions exhibit a "solid-crossing" column structure that is commonly observed in Pd(dmit)$_2$ anion radical salts, in which the two anion layers are different in terms of the stacking direction.[2] Several intermolecular S···S contacts are observed within each layer, while no contacts are detected between the layers **A** and **B**. The anion layers are isolated from each other by the cation layer. These results reveal that **1** is a new *bilayer system*, and the anion arrangement in both layers differs from that in the bilayer salt (Me-3,5-DIP)[Ni(dmit)$_2$]$_2$.[12a] The anion arrangement viewed along the molecular long axis (end-on projection) is shown in Figure 3, and the anion···anion overlap integrals among the LUMOs of Ni(dmit)$_2$ are listed in Table 3. In layer **A**, the overlap integrals **a** and **b** are larger than the others, and **a** is approximately 5 times larger than **b**. This indicates that the anions are dimerized and the dimers are stacked along the ***a***+***c*** direction to form a 1D electronic network. The anisotropic nature is expected to be reduced in layer **B**, in which the anions are weakly dimerized along the stacking direction (***a***-axis) with moderate overlap integral values along the diagonal direction (**p**, **r**).

The electronic band structure was calculated for each layer based on the tight-binding approximation, and the results are shown in Figures 3c and d. In layer **A**, the LUMO band consists of upper and lower bands separated by an energy gap (ΔE_g = 0.27 eV), because of strong dimerization of the anions. The widths of both the upper and the lower bands (0.11 eV) are smaller than ΔE_g. The LUMO band should be totally 1/4-filled by considering the [Ni(dmit)$_2$]$^{-0.5}$ charge state of anion **A**, and thus the Fermi level ε_F is located across the lower band. Consequently, an effectively half-filled (1/2-filled) state is realized. The narrow bandwidth and half-filled nature of the lower band suggest that layer **A** forms a Mott insulating state, as similarly observed in one of the two anion layers of (Me-3,5-DIP)[Ni(dmit)$_2$]$_2$.[12a] In this case, one electron (S = 1/2 spin) locates at one [Ni(dmit)$_2$]$_2^-$ unit. The calculated Fermi surface represents the one-dimensional (1D) character of layer **A** (Figure 3e). For layer **B**, the LUMO band is also separated into upper and lower bands by a dimerization gap, and the lower band is effectively half-filled. The widths of the upper and lower bands are larger, and the energy gap is smaller than those in layer **A**. This situation originates from the smaller intradimer overlap integral (**a**) and the larger interdimer overlap integral along the stacking direction (**b**), in addition to the larger overlap integrals along the diagonal direction (**p**, **r**). The Fermi surface is open along the ***a**** direction, but is largely distorted, which means that a two-dimensional (2D) character is enhanced (Figure 3f). All these results suggest that layer **B** is in a weaker Mott insulating state. The crystal and electronic structures, together with the conducting and magnetic properties reported later, indicate that **1** is a novel *bilayer Mott insulator*, in which both anion layers **A** and **B** are in a Mott insulating state. It should be emphasized that the two independent anion layers **A** and **B** differ markedly in their band dispersion and width; however, their fillings are identical (effectively half-filled). This situation is in sharp contrast to that

dx.doi.org/10.1021/ic301552z | *Inorg. Chem.* 2012, 51, 11645−11654

Table 1. Crystal Data and Refinement Parameters for (Et-2,5-DBrP)Br·H_2O, (Et-2,5-DBrP)[Ni(dmit)$_2$]$_2$ (1), (Et-2I-5BrP)[Ni(dmit)$_2$]$_2$ (2), and (Et-2Br-5IP)[Ni(dmit)$_2$]$_2$ (3)

	(Et-2,5-DBrP)Br·H_2O	(Et-2,5-DBrP)[Ni(dmit)$_2$]$_2$ (1)	(Et-2I-5BrP)[Ni(dmit)$_2$]$_2$ (2)	(Et-2Br-5IP)[Ni(dmit)$_2$]$_2$ (3)
empirical formula	$C_7H_{10}Br_3NO$	$C_{19}H_8Br_2NNi_2S_{20}$	$C_{19}H_8BrINNi_2S_{20}$	$C_{19}H_8BrINNi_2S_{20}$
Fw	363.86	1168.7	1215.69	1215.69
crystal dimension (mm^3)	0.30 × 0.10 × 0.05	0.2 × 0.1 × 0.03	0.15 × 0.06 × 0.03	0.2 × 0.15 × 0.04
crystal system	triclinic	triclinic	triclinic	triclinic
a (Å)	11.530(5)	7.560(2)	7.4236(4)	12.036(11)
b (Å)	13.106(7)	38.912(15)	39.197(2)	20.100(18)
c (Å)	7.787(4)	6.516(2)	6.4439(3)	7.826(7)
α (deg)	90.238(11)	94.527(9)	94.175(3)	90.293(8)
β (deg)	109.523(11)	112.330(8)	112.764(3)	101.977(14)
γ (deg)	89.239(10)	85.678(10)	85.971(3)	104.356(6)
V (Å^3)	1108.9(9)	1765(1)	1722.6(2)	1791(3)
space group	$P\bar{1}$	$P\bar{1}$	$P\bar{1}$	$P\bar{1}$
Z value	4	2	2	2
λ (Å)	0.7107	0.7107	0.7107	0.7107
T (K)	293	293	93	293
μ (Mo Kα) (mm^{-1})	10.872	4.534	4.383	4.216
D_{calc} (g/cm^3)	2.180	2.198	2.344	2.254
R_1	0.0378	0.0713	0.0636	0.0576
wR_2	0.0891	0.1821	0.1538	0.1465
goodness of fit	0.999	1.036	1.201	0.811

Table 2. Average Bond Lengths in Ni(dmit)$_2$ Anions in Each Salt (LUMO of Ni(dmit)$_2$ Is Shown)[a]

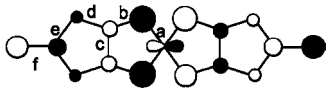

complex	anion	a	b	c	d	e	f
1	A	2.163	1.700	1.355	1.752	1.732	1.645
	B	2.166	1.706	1.365	1.742	1.726	1.652
2	A	2.160	1.701	1.363	1.742	1.728	1.650
	B	2.156	1.703	1.372	1.736	1.728	1.654
3	A	2.163	1.688	1.358	1.758	1.746	1.625
	B	2.156	1.712	1.376	1.726	1.729	1.651
Ni(dmit)$_2^{0}$[14]		2.143	1.69	1.393	1.735	1.739	1.635
Ni(dmit)$_2^{-1}$[15]		2.206	1.742	1.377	1.737	1.726	2.052

[a]Errors: ±0.01 Å for Et-2,5-DBrP salt; ±0.01 Å for Et-2Br5IP salt; ±0.007−0.009 Å for Et-2I5BrP salt.

reported for the bilayer salt $(Me_3Te)[Ni(dmit)_2]_2$, in which the two different energy bands originated from the two independent anion layers exhibit different band filling.[11] These differences represent the diversity of Ni(dmit)$_2$ in terms of its oxidation state, molecular arrangement, and electronic structure.

The halogen bond between the cation and the anion is a possible factor to obtain the bilayer structure. We investigated the effect of the halogen bond on the construction of the bilayer structure by replacing one Br atom with an I atom in the Et-2,5-DBrP cation. The I atom acts as a stronger halogen bond donor than the Br atom.[16] As shown in Figure 2a, the Br···S halogen bonds are formed at the 2-position in the cation, while it is not formed at the 5-position. Therefore, the introduction of I atom at the different positions (2- or 5-position) is expected to induce different halogen bond formations, and thus different crystal structures.

Crystal and Electronic Structures of (Et-2I-5BrP)[Ni(dmit)$_2$]$_2$ (2). The crystal of (Et-2I-5BrP)[Ni(dmit)$_2$]$_2$ (**2**), in which the Et-2I-5BrP cation has an I atom at the 2-position and a Br atom at the 5-position, appeared as an assembly of overlaid thin plates. This made the crystal structure analysis difficult. Analysis of the crystal structure of **2** with acceptable data accuracy was achieved by cutting the overlaid plates into a small single crystal and collecting the data at 93 K using a confocal mirror system.

The crystal structure of **2** depicted in Figure 4 is isostructural with (Et-2,5-DBrP)[Ni(dmit)$_2$]$_2$ (**1**). The crystal contains two crystallographically independent Ni(dmit)$_2$ anions **A** and **B**, and one crystallographically independent Et-2I-5BrP cation. The I···S and Br···S distances between the cation and the anions **A** and **B** are short. (Figure 4a). However, these halogen···S distances cannot be compared directly with the van der Waals radii of S, Br, and I atoms determined at room temperature because the crystal structure was analyzed at 93 K. Nevertheless, the observed I···S distance (3.167(2) Å) is much shorter than the sum of the van der Waals radii of S and I atoms (3.78 Å), which indicates the strong nature of the I···S halogen bond. The bond lengths in the anions **A** and **B** were almost identical (Table 2), which implies the $[Ni(dmit)_2]^{-0.5}$ oxidation state in both anions, similar to that for **1**. Each anion constructs an independent layer as shown in Figures 4b and c, which provides evidence for the bilayer character of **2**.

dx.doi.org/10.1021/ic301552z | Inorg. Chem. 2012, 51, 11645−11654

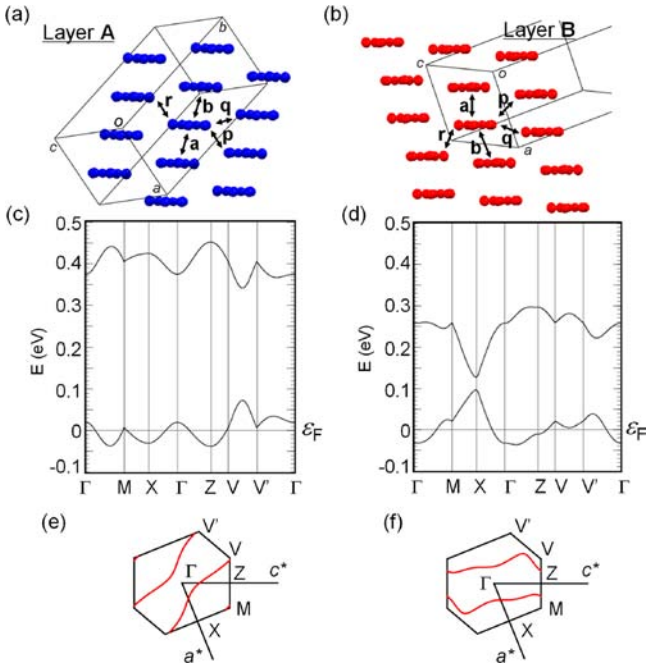

Figure 3. Anion arrangement of (Et-2,5-DBrP)[Ni(dmit)$_2$]$_2$ (**1**) viewed along the molecular long axis within the layers **A** (a) and **B** (b). Calculated band structures for the layers **A** (c) and **B** (d), and Fermi surfaces for the layers **A** (e) and **B** (f). **a**, **b**, **p**, **q**, **r** in (a) and (b) correspond to the directions of overlap integrals listed in Table 3.

The overlap integrals among the LUMOs of Ni(dmit)$_2$ are indicated in Figure 3 and Table 3. As observed for **1**, the anion is dimerized in layer **A**, and the dimers are stacked along the ***a*** **+*c*** direction to form a 1D electronic structure. In layer **B**, the dimerized anions form a less 1D electronic network through moderate overlap integrals along the transverse direction (**p**, **r**). Note that all the overlap integrals except **p** in layer **A** are larger in **2** than in **1**, despite the introduction of an I atom, which is larger than the Br atom, into **2**. This tendency is due to the difference in the temperature at which the single crystal XRD analysis was conducted; 93 K for **2** and 293 K for **1**. As the temperature is decreased, the crystal lattice shrinks because of suppression of the thermal vibration of atoms and the lattice, which causes the overlap integrals in **2** to be larger than those in **1**.

The band structure and Fermi surface of each layer in **2** are depicted in Supporting Information, Figure S2, and are almost identical to those of **1**. Layer **A** has a narrow band and 1D Fermi surface, while layer **B** forms a wider band with a largely distorted planar Fermi surface. Both conduction bands are effectively half-filled, which suggests that **2** is a second example of a *bilayer Mott insulator*. The electronic character is confirmed by investigation of the electrical and magnetic properties.

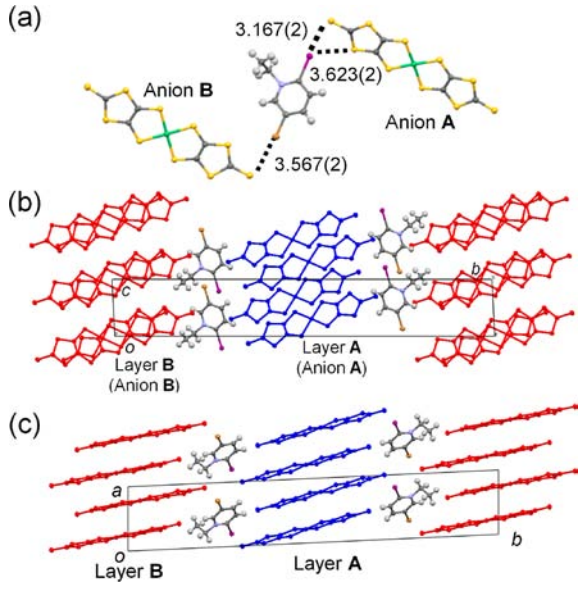

Figure 4. Crystal structure of (Et-2I-5BrP)[Ni(dmit)$_2$]$_2$ (**2**): Crystallographically independent anions and cation. Halogen···S distances (Å) are depicted as dotted lines (a). Views along the ***a***-axis (b), and along the ***c***-axis (c).

Crystal and Electronic Structures of (Et-2Br-5IP)[Ni(dmit)$_2$]$_2$ (3). The crystal structure of (Et-2Br-5IP)[Ni(dmit)$_2$]$_2$ (**3**), in which the Et-2Br-5IP cation contains an I atom at the 5-position and a Br atom at the 2-position, is shown in Figure 5. The crystal structure is markedly different from those of (Et-2,5-DBrP)[Ni(dmit)$_2$]$_2$ (**1**) and (Et-2I-5BrP)[Ni(dmit)$_2$]$_2$ (**2**). The unit cell contains two crystallographically independent Ni(dmit)$_2$ anions **A** and **B**, and one Et-2Br-5IP cation. In addition to a Br···S halogen bond between the 2-position in the cation and the anion, similar to that in **1**, there are I···S halogen bonds at the 5-position in the cation. The introduction of the I atom provides additional halogen bond formation, which induces significant structural changes.[24] The anion **A** is slightly bent along the molecular long axis, while the anion **B** is planar. The bond lengths of the anions **A** and **B** are similar, as listed in Table 2, which suggests an equivalent oxidation state ([Ni(dmit)$_2$]$^{-0.5}$ state) of the anions. The anions stack along the ***-a*+*c*** direction with **−A−A−B−B−** manner, in which the formation of **A−A** and **B−B** dimers is revealed by the calculated overlap integrals (Table 3). The anion stack is arranged along the ***a***-axis to form a 2D anion layer. Weak interstack overlap integrals (**p**, **q**, **r**, **s**) along the ***a***-axis, however, result in a 1D rather than 2D electronic structure. The anion layer is separated by the cation layer along the ***b***-axis, and no interlayer $S_{anion}\cdots S_{anion}$ contact is evident. This salt, where only one kind of anion layer is present in the unit cell, is a *monolayer system*. The anion column has 4-fold periodicity

Table 3. Overlap Integrals $S \times 10^{-3}$ between Two Anions in Each Salt[a]

compound		a	b	c	p	q	r	s	t
1	layer A	−19.6	4.01		−0.64	0.25	−1.52		
	layer B	11.3	3.62		−3.28	0.76	2.85		
2	layer A	−22.6	5.41		−0.55	0.36	−2.20		
	layer B	13.7	4.79		−4.17	0.8	3.41		
3		−21.3	−1.05	10.8	−2.93	−0.37	0	−0.74	1.96

[a] a, b, c, p, q, r, s, t correspond to those in Figures 3 and 6.

dx.doi.org/10.1021/ic301552z | *Inorg. Chem.* 2012, 51, 11645−11654

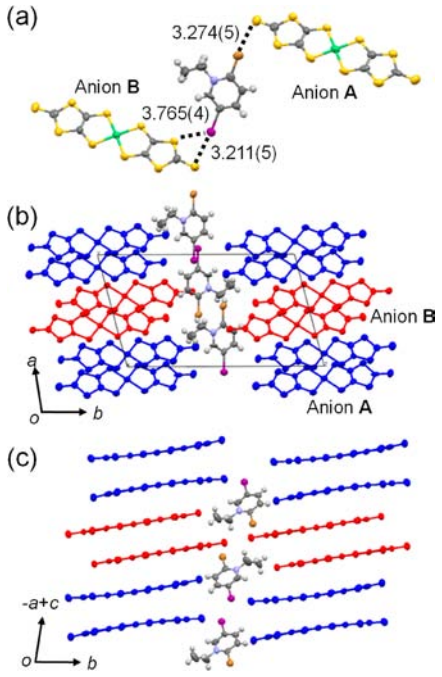

Figure 5. Crystal structure of (Et-2Br-5IP)[Ni(dmit)$_2$]$_2$ (**3**): Crystallographically independent anions and cation. Halogen bonds are depicted as dotted lines (a). View along the *c*-axis (b) and anion stacking mode along the *-a+c* direction (c).

and the energy band is 1/4-filled, which leads the system into a band insulating state. The band insulating nature is confirmed by the calculated band structure shown in Figure 6b, and is

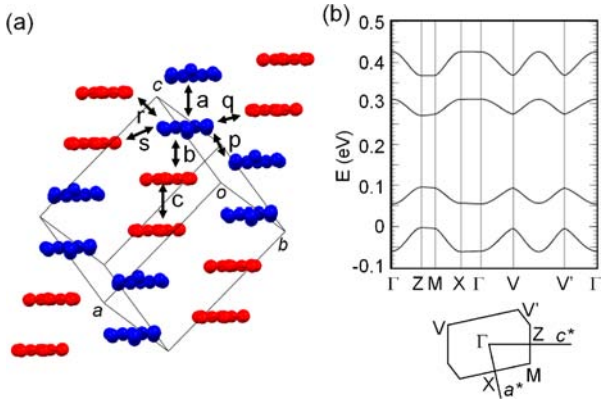

Figure 6. Anion arrangement of (Et-2Br-5IP)[Ni(dmit)$_2$]$_2$ (**3**) viewed along the molecular long axis (a), and calculated band structure (b). **a**, **b**, **c**, **p**, **q**, **r**, **s** in (a) indicate the overlap integrals listed in Table 3.

consistent with the transport properties reported later. The structural studies of **1**, **2**, and **3** have revealed that the crystal structure can be controlled by selective tuning of the halogen bond strength. Therefore, the halogen bond between the cation and the anion plays a major role in determining the crystal structure, and the introduction of cation···anion supramolecular interaction is an attractive approach to realize a bilayer structure.

Electrical Transport Properties of 1, 2, and 3. The electrical resistivity parallel to the anion layers was measured for (Et-2,5-DBrP)[Ni(dmit)$_2$]$_2$ (**1**), (Et-2I-5BrP)[Ni(dmit)$_2$]$_2$ (**2**), and (Et-2Br-5IP)[Ni(dmit)$_2$]$_2$ (**3**) using the standard four-probe method. The results are shown in Figure 7.

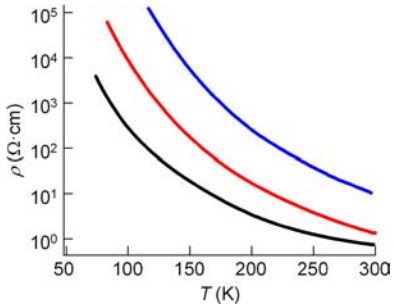

Figure 7. Temperature dependence of resistivity ρ of (Et-2,5-DBrP)[Ni(dmit)$_2$]$_2$ (**1**) (black), (Et-2I-5BrP)[Ni(dmit)$_2$]$_2$ (**2**) (red), and (Et-2Br-5IP)[Ni(dmit)$_2$]$_2$ (**3**) (blue).

The isostructural salts **1** and **2** display semiconducting behavior, and the resistivity ρ increases with decreasing temperature. The semiconducting characteristics support the bilayer Mott insulating nature of both salts **1** and **2**, where the charge carriers are localized on each anion dimer [Ni(dmit)$_2$]$_2^-$. These electrical properties contrast with those of the bilayer salt (Me-3,5-DIP)[Ni(dmit)$_2$]$_2$, in which the anions are arranged in a spanning-overlap mode to achieve 2D metallic conduction within one of the two anion layers.[12a] The observed electrical properties of **1** and **2** are mainly due to the anion layer **B**, which has a smaller energy gap and wider conduction bandwidth than the layer **A** (Figure 3 and Supporting Information, Figure S2). The room temperature electrical conductivity σ_{RT}, of **1** is 2 S·cm^{-1}, and the activation energies, E_a, are 40 meV (>150 K) and 27 meV (<150 K), while for **2**, σ_{RT} = 0.3 S·cm^{-1} and E_a = 56 meV (>150 K) and 37 meV (<150 K). The difference reflects the weaker anion−anion interaction in the layer **B** of **2** than of **1**, which is presumably due to a negative chemical pressure effect. The introduction of the I atom in **2** expands the crystal lattice, accompanied by elongation of the anion···anion distance, which eventually decreases the anion−anion interactions (overlap integrals). ρ under pressure was investigated for **1** up to 0.3 GPa, where ρ and E_a increased with increasing pressure (Supporting Information, Figure S3).

The temperature dependence of ρ is semiconducting for **3** with σ_{RT} = 0.1 S·cm^{-1} and E_a = 70 meV. This result is in agreement with the band insulating characteristics of **3** indicated by the band structure calculation.

Magnetic Properties of 1 and 2. The magnetic properties of (Et-2,5-DBrP)[Ni(dmit)$_2$]$_2$ (**1**) and (Et-2I-5BrP)[Ni(dmit)$_2$]$_2$ (**2**) were investigated using a superconducting quantum interference device (SQUID) magnetometer and electron spin resonance (ESR) spectroscopy. A Mott insulator has spin degree of freedom and displays diverse magnetic properties.

The temperature-dependent magnetic susceptibility of **1** measured at 10 kOe is shown in Figure 8a. χ increases and χT decreases with decreasing temperature from 300 K. The room temperature χ of 1.26 × 10^{-3} emu·mol^{-1} is close to that expected for a state where one S = 1/2 spin is localized on every [Ni(dmit)$_2$]$_2^-$ unit in both anion layers **A** and **B** (1.31 × 10^{-3} emu·mol^{-1}); however, it is much larger than that for conventional Pauli paramagnetism (≈4.0 × 10^{-4} emu·mol^{-1}). In the temperature range from 300 to 30 K, χT can be analyzed

dx.doi.org/10.1021/ic301552z | Inorg. Chem. 2012, 51, 11645−11654

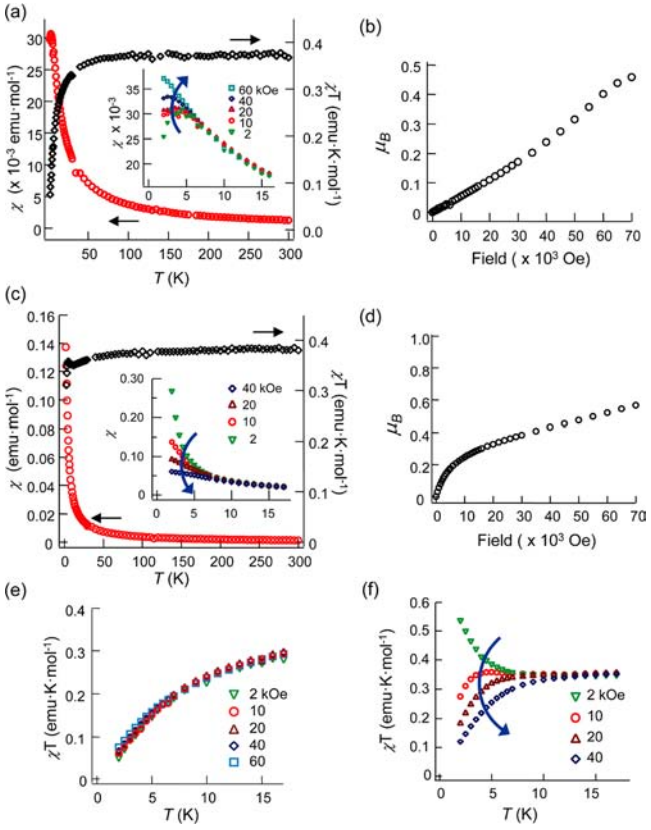

Figure 8. Temperature dependence of magnetic susceptibility χ (red circle) and χT product (black diamond) at 10 kOe of (Et-2,5-DBrP)$[Ni(dmit)_2]_2$ (**1**) (a) and (Et-2I-5BrP)$[Ni(dmit)_2]_2$ (**2**) (c), and magnetization curve at 2 K of **1** (b) and **2** (d), and magnetic field dependence of χT of **1** (e) and **2** (f). Insets in (a) and (c) show the magnetic field dependence of χ.

by the Curie–Weiss law to yield a Curie constant, C, of 0.386 emu·K·mol^{-1} and a Weiss temperature, θ, of −4.9 K. The C value is almost identical to that estimated for one $S = 1/2$ spin on one $[Ni(dmit)_2]_2^-$ unit (0.392 emu·K·mol^{-1} with g = 2.046). This result confirms that **1** is a *bilayer Mott system*, where the spin is localized on the $[Ni(dmit)_2]_2^-$ unit in both layers **A** and **B**. The negative θ suggests a dominant antiferromagnetic (AFM) interaction between the spins. Below 10 K, χ shows a maximum at 5.5 K, below which χ decreases with decreasing temperature. The inset of Figure 8a shows the χ dependency on the applied magnetic field, where χ increases with the magnetic field and spin-flop like behavior is observed around 20 to 40 kOe. The magnetization measured at 2 K is displayed in Figure 8b and increases with the magnetic field, accompanied by the appearance of spin flop-like behavior at about 35 kOe. The magnetization does not saturate, but reaches about 0.5 μ_B at 70 kOe. These results indicate the presence of strong AFM interaction between the spins at 2K. However, heat capacity measurements suggest the absence of 3D long-range magnetic ordering down to 0.6 K (Supporting Information, Figure S4). ESR measurements were conducted for **1** (Supporting Information, Figure S5); the g-value and ΔH_{pp} decrease with temperature, and below 20 K, the g-value abruptly decreases and ΔH_{pp} broadens, which is typical behavior of short-range AFM ordering. Therefore, the spins are strongly coupled to form short-range AFM ordering within the layers. The appearance of the maximum χ value at 5.5 K is presumably due to the significant evolution of short-range AFM ordered domains.[25]

The magnetic behavior of **2** (Figure 8c) above 30 K can be described by the Curie–Weiss law with C = 0.382 emu·K·mol^{-1} and θ = −1.8 K. The C value obtained indicates that, similarly to **1**, one $S = 1/2$ spin is localized on one $[Ni(dmit)_2]_2^-$ unit. The negative θ indicates the presence of AFM interaction between the spins, and the smaller θ for **2** than that for **1** suggests weaker anion–anion interactions. These results are due to the negative chemical pressure effect for **2**, as discussed with regard to the conducting properties. These results provide evidence for the bilayer Mott insulating nature of **2**. ESR measurements for **2** revealed similar g-value and ΔH_{pp} temperature dependence to that for **1**, which indicates strong AFM coupling of the spins to develop short-range AFM ordering below 16 K.[17] The magnetic properties of **2** are markedly different from those of **1** below 10 K; while χ continues to increase down to 2 K at 10 kOe for **2**, χ has a maximum at 5.5 K for **1**. χ exhibits magnetic field dependence below 7 K, in which χ decreases with increasing magnetic field (inset of Figure 8c). This behavior is in sharp contrast with that for **1**, in which χ increases with the magnetic field (inset of Figure 8a). χT also exhibits characteristic magnetic field dependence below 15 K for **2**, which is not observed for **1** (Figures 8e and f). The χT versus T plot shows ferromagnetic (FM)-like behavior at 2 kOe, in which χT increases below 7.5 K; however, the FM-like behavior becomes AFM with increasing magnetic field. As shown in Figure 8d, the magnetization of **2** increases sharply with the magnetic field up to 10 kOe, above which the increase becomes gradual. The magnetization does not saturate but reaches about 0.6 μ_B at 70 kOe.[25] It is noted that no hysteresis and crystal-axis dependence[18] are observed in the magnetization curve. These results suggest that several types of magnetic interactions, including FM and AFM interactions, are competing in **2**, which results in the complex magnetic behavior.

It is interesting that the isostructural salts **1** and **2** demonstrate contrasting magnetic behavior in the low temperature region. We have focused on the intralayer and interlayer spin–spin interactions in these two salts to interpret their magnetic behavior. Each salt contains two different types of Mott insulating layers (layers **A** and **B**, as shown in Figures 2 and 4), in which intralayer AFM exchange interactions are dominant in both layers. Layers **A** and **B** are spatially and magnetically separated by the cation layers, so that 3D long-range magnetic ordering is suppressed and short-range AFM ordered domains should grow within the layers. Therefore, a small but non-negligible amount of fluctuated spins that do not participate in the formation of the AFM domains can exist at the borders or outside of the domains (Figure 9). Indeed, heat capacity measurements revealed that such kind of spins are present (17 ± 3%) in both **1** and **2** (Supporting Information, Figure S4). These fluctuated spins influence the low temperature magnetic behavior.

The fluctuated spins in **1** are considered to couple antiferromagnetically, and **1** demonstrates overall AFM behavior. This indicates the interlayer AFM exchange interaction as shown in Figure 9. In contrast, the fluctuated spins in **2** should be coupled ferromagnetically to exhibit the FM-like magnetic anomaly. Thus, the interlayer exchange interaction should be FM in **2**, which is in sharp contrast with the interlayer AFM interaction in **1**. The interlayer interaction is based on a superexchange mechanism mediated by the

dx.doi.org/10.1021/ic301552z | Inorg. Chem. 2012, 51, 11645–11654

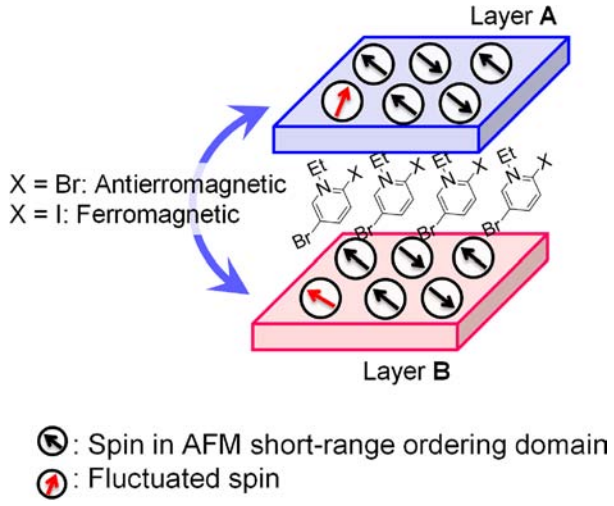

Figure 9. Expected magnetic structures for **1** (X = Br) and **2** (X = I).

cations that is sensitive to the types and steric arrangements of the atoms and orbitals involved. In the present system, the halogen atoms in the cation are associated with the interlayer interaction through cation···anion halogen bonds, while **1** and **2** have different halogen atoms at the 2-position of the cation. Therefore, this difference is the main cause of the different magnetic properties exhibited by **1** and **2**.

In both salts, 3D long-range magnetic ordering is suppressed by the low dimensionality of the anion layers, which results in the development of short-range AFM ordered domains within the layers in the low temperature region. This gives rise to the generation of fluctuated spins, which are considered to be the main cause for the observed magnetic behavior of **1** and **2** below 10 K. Such fluctuated spins are expected to be sensitive to external stimuli, and thus can result in unique magnetic or magneto-conducting properties. The generation of fluctuated spins causes magnetic inhomogeneity in each layer, which further suppresses the development of long-range magnetic ordering. It is expected that the bilayer system yields fluctuated spins more easily than the monolayer system. The two layers with different spin arrangements and magnetic inhomogeneity are aligned alternately, and all the layers are sandwiched by insulating layers (cation layers) in the bilayer system; therefore, the development of spin-correlation along the interlayer direction, which induces long-range magnetic ordering, is suppressed more strongly in the bilayer system than in the monolayer system.

CONCLUSION

A new bilayer $Ni(dmit)_2$ anion radical salt, (Et-2,5-DBrP)[$Ni(dmit)_2]_2$ (**1**), was developed. Single crystal XRD analysis revealed $Br_{cation}\cdots S_{anion}$ halogen bonds in the crystal. Band structure calculations suggest that **1** is a novel *bilayer Mott insulator*, in which two different types of Mott-insulating anion layers (**A** and **B**) coexist in one crystal. The bilayer Mott insulating character was confirmed by investigation of the conducting and magnetic properties. Selective halogen substitution of a Br atom for an I atom at the 2-position in the cation afforded another new bilayer salt (Et-2I-5BrP)[$Ni(dmit)_2]_2$ (**2**), which is isostructural with **1**, while substitution at the 5-position caused a structural change to yield a monolayer salt, (Et-2Br-5IP)[$Ni(dmit)_2]_2$ (**3**). The results indicate that the halogen bond plays an important role to realize a bilayer system, and that the crystal structure can be controlled by tuning the strength of the halogen bond. Resistivity measurements of **1**, **2**, and **3** revealed semiconducting characteristics. Magnetic studies of **1** and **2** revealed a marked difference in their low temperature magnetic properties, which are affected by fluctuated spins that do not participate in the formation of the short-range AFM ordered domains. Such fluctuated spins, which are generated more easily in the bilayer system than in the monolayer system, are expected to result in unique physical properties.

EXPERIMENTAL SECTION

Materials. Solvents and reagents were used as received from commercial sources unless noted otherwise. ($^nBu_4N$)[$Ni(dmit)_2$] was prepared according to the literature.[19] Halogenated pyridines were purchased from Aldrich, and $Et_3O{\cdot}BF_4$ was from TCI. All syntheses were performed under Ar atmosphere.

Synthesis of (dihalo-pyridiium)BF_4. The mixture of corresponding dihalo-pyridine (1 g) and Et_3OBF_4 (1.3 equiv) in CH_3CN 100 mL was stirred overnight at room temperature. Solvent was removed by rotary evaporator, and the resulting solids were washed with CH_2Cl_2 (15 mL) and small amount of acetone (few drops) by ultrasonication. The residue was filtered, and the precipitate was recrystallized from CH_3CN-Et_2O (two times) to yield (dihalo-pyridiium)BF_4.

(Et-2,5-DBrP)BF_4: Yield: 32%. Anal. Calcd for $C_7H_8BBr_2F_4N$: C, 23.83; H, 2.29; N, 3.97. Found: C, 23.88; H, 2.31; N, 3.90. ^{1}H NMR (DMF-d^6): δ 1.51 (t, 3H, J = 7.2 Hz), 4.70 (q, 4H, J = 7.2 Hz), 8.45 (dd, 1H, J = 1.8 Hz, 8.4 Hz), 8.72 (dd, 1H, J = 1.8 Hz, 9.0 Hz), 9.64 (d, 1H, J = 1.8 Hz). MS (ESI-TOF+): m/z 266 [Et-2,5-DBrP]$^+$.

(Et-2I-5BrP)BF_4: Yield: 42%. Anal. Calcd for $C_7H_8BBrF_4IN$: C, 21.03; H, 2.02; N, 3.50. Found: C, 21.04; H, 2.03; N, 3.44. ^{1}H NMR (DMF-d^6): δ 1.49 (t, 3H, J = 7.2 Hz), 4.69 (q, 4H, J = 7.2 Hz), 8.42 (dd, 1H, J = 2.1 Hz, 8.4 Hz), 8.68 (d, 1H, J = 1.8 Hz, 8.4 Hz), 9.68 (d, 1H, J = 2.1 Hz). MS (ESI-TOF+): m/z 312 [Et-2I-5BrP]$^+$.

(Et-2Br-5IP)BF_4: Yield: 38%. Anal. Calcd for $C_7H_8BBrF_4IN$: C, 21.03; H, 2.02; N, 3.50. Found: C, 21.13; H, 2.12; N, 3.50. ^{1}H NMR (DMF-d^6): δ 1.49 (t, 3H, J = 7.2 Hz), 4.67 (q, 4H, J = 7.2 Hz), 8.42 (d, 1H, J = 9.0 Hz), 8.68 (d, 1H, J = 9.0 Hz), 9.60 (d, 1H, J = 2.1 Hz). MS (ESI-TOF+): m/z 312 [Et-2Br-5IP]$^+$.

Synthesis of Anion Radical Salts (dihalo-pyridiium)[Ni(dmit)$_2$]$_2$. Single crystals of (Et-2,5-DBrP)[$Ni(dmit)_2]_2$ (**1**), (Et-2I-5BrP)[$Ni(dmit)_2]_2$ (**2**), and (Et-2Br-5IP)[$Ni(dmit)_2]_2$ (**3**) and (**4**) were obtained by galvanostatic electrolysis of a mixture of ($^nBu_4N$)-[$Ni(dmit)_2$] (3−4 mg) and a large excess of (dihalo-pyridiium)BF_4 as supporting electrolyte (40−50 mg) in 20 mL of acetone or a mixture of acetone and acetonitrile (1:1, v/v) under Ar. An H-shaped 20 mL cell and Pt electrodes (1 mm diameter) were used, and a constant current of 0.3 μA was applied for a week at 20 °C.

NMR Spectroscopy. ^{1}H NMR spectra were recorded with a JEOL AL-300 spectrometer. Sample was dissolved in deutrated DMF (DMF-d^6). Solvent residual peak was set at δ = 2.5 as an internal reference.

Single Crystal X-ray Diffraction Analysis. The data for (Et-2,5-DBrP)Br·H_2O, **1**, and **3** were collected at room temperature on a Rigaku AFC-7R diffractometer with a Rigaku Mercury CCD system equipped with a rotating-anode X-ray generator that emits graphite-monochromated Mo Kα radiation (0.7107 Å). A suitable single crystal was mounted on a looped film (micromount) with grease. An empirical absorption correction using equivalent reflections and Lorentzian polarization correction was performed with the program Crystal Clear 1.3.6. The structure was solved with SIR-92, and the whole structure was refined against F^2 using SHELXL-97.[20] All non-hydrogen atoms were refined anisotropically. Hydrogen atoms were located in idealized positions and were refined using a riding model with fixed thermal parameters.

The data for **2** were collected at 93 K on a Rigaku AFC-8 diffractometer equipped with a Saturn70 CCD detector using Mo Kα radiation by an ω-scan method with 0.5° oscillation for each frame. X-ray was monochromated and focused by a confocal mirror. Bragg spots

were integrated using the HKL2000 program package,[21] and Lorentz and polarization but no absorption corrections were applied. The structure was solved with SIR-92, and the whole structure was refined against F^2 using SHELXL-97.[20] All non-hydrogen atoms were refined anisotropically. Hydrogen atoms were located in idealized positions and were refined using a riding model with fixed thermal parameters.

Pertinent crystallographic data were given in Table 1.

Resistivity Measurements. The direct-current resistivity measurements were performed with single crystals of **1**, **2**, and **3** using the standard four-probe method. Electrical contacts were obtained by gluing four gold wires (15 mm diameter) to the crystal with carbon paste.

Band Calculations. The LUMO was obtained by extended Hückel MO calculation.[22] The calculation was carried out with the use of semiempirical parameters for Slater-type atomic orbitals listed in ref 10. Double-ζ orbitals were used for Ni. Band calculations were performed under the tight-binding approximation. Transfer integrals (t) were approximated from overlap integrals (S) via the formula $t \approx \varepsilon S$ (ε is a constant whose order is the one of the energy level of the LUMO: $\varepsilon = -10$ eV).[23] For **1** and **2**, the band structures for the two different anion layers were calculated individually, and the Fermi energy ε_f for each layer was set at 1/4-filled position.

ESR Measurements. The ESR spectra were collected for **1** and **2** using a JEOL JES-RE2X. The plate crystals were attached to the planar surface on a quartz rod with the crystal plane parallel to the quartz surface. The magnetic field was applied approximately perpendicular to the crystal plane (***bc***-plane).

Magnetic Measurements by SQUID. The temperature dependence of the magnetic susceptibility of **1** and **2** was measured with a Quantum Design MPMS SQUID magnetometer. Aluminum foil was used as a sample container, whose magnetic contribution was subtracted as background by measuring its own magnetic susceptibilities in every measurement. The diamagnetic correction χ_{dia} for the sample was carried out with Pascal's constants. χ_{dia}: 5.03×10^{-4} emu·mol^{-1} for **1**; 5.17×10^{-4} emu·mol^{-1} for **2**.

■ ASSOCIATED CONTENT

Ⓢ Supporting Information

Crystal structure of **4**, band structure of **2**, resistivity of **1** under pressure, and magnetic heat capacity of **1** and **2**. This material is available free of charge via the Internet at http://pubs.acs.org.

■ AUTHOR INFORMATION

Corresponding Author

*E-mail: kusamoto@riken.jp.

Present Addresses

[†]Institute for Molecular Science, Nishigonaka 38, Myodaiji, Okazaki 444-8585, Japan.

[‡]PRESTO, Japan Science and Technology Agency, Honcho Kawaguchi, Saitama 332-0012, Japan.

[§]Department of Physics, Toho University, Miyama 2-2-1, Funabashi-shi, Chiba 274-8510, Japan.

[∥]Department of Chemistry, Graduate School of Science, Osaka University, Machikaneyama 1-1, Toyonaka, Osaka 560-0043, Japan.

Notes

The authors declare no competing financial interest.

■ ACKNOWLEDGMENTS

We thank Dr. Daisuke Hashizume for help in single crystal XRD study of **2**. This research was partially supported by Grant-in-Aid for Scientific Research (S) (No. 22224006) from the Japan Society for the Promotion of Science (JSPS). Y.O. acknowledges the support by the Grant-in-Aid for Scientific Research on Innovative Areas (No.20110004) from the Ministry of Education, Science, Sports and Culture, Japan.

■ REFERENCES

(1) (a) Stiefel, E. I.; Karlin, K. D. *Progress in Inorganic Chemistry, Dithiolene Chemistry: Synthesis, Properties, and Applications*; Wiley-Interscience: New York, 2003; Vol. *52*. (b) Kobayashi, A.; Fujiwara, E.; Kobayashi, H. *Chem. Rev.* **2004**, *104*, 5243−5264. (c) Kobayashi, A.; Okano, Y.; Kobayashi, H. *J. Phys. Soc. Jpn.* **2006**, *75*, 051002/1−051002/12.

(2) (a) Kato, R. *Chem. Rev.* **2004**, *104*, 5319−5346. (b) Cassoux, P. *Coord. Chem. Rev.* **1999**, *185*−*86*, 213−232. (c) Akutagawa, T.; Nakamura, T. *Coord. Chem. Rev.* **2000**, *198*, 297−311. (d) Tamura, M.; Kato, R. *Sci. Technol. Adv. Mater.* **2009**, *10*, 024304. (e) Kanoda, K.; Kato, R. *Annu. Rev. Condens. Matter Phys.* **2011**, *2*, 167−188.

(3) (a) Canadell, E. *New J. Chem.* **1997**, *21*, 1147. (b) Tajima, H.; Naito, T.; Tamura, M.; Kobayashi, A.; Kuroda, H.; Kato, R.; Kobayashi, H.; Clark, R. A.; Underhill, A. E. *Solid State Commun.* **1991**, *79*, 337−341. (c) Miyazaki, T.; Ohno, T. *Phys. Rev. B* **1999**, *59*, R5269−R5272.

(4) Mott, N. F. *Metal-Insulator Transitions*; Taylor & Francis: Oxford, U.K., 1990.

(5) Tamura, M.; Kato, R. *J. Phys.: Condens. Matter* **2002**, *14*, L729−L734.

(6) (a) Tamura, M.; Kato, R. *Chem. Phys. Lett.* **2004**, *387*, 448−452. (b) Nakao, A.; Kato, R. *J. Phys. Soc. Jpn.* **2005**, *74*, 2754−2763. (c) Tamura, M.; Takenaka, K.; Takagi, H.; Sugai, S.; Tajima, A.; Kato, R. *Chem. Phys. Lett.* **2005**, *411*, 133−137.

(7) (a) Tamura, M.; Nakao, A.; Kato, R. *J. Phys. Soc. Jpn.* **2006**, *75*, 093701/1−093701/4. (b) Kato, R.; Tajima, A.; Nakao, A.; Tamura, M. *J. Am. Chem. Soc.* **2006**, *128*, 10016−10017. (c) Shimizu, Y.; Akimoto, H.; Tsujii, H.; Tajima, A.; Kato, R. *Phys. Rev. Lett.* **2007**, *99*, 256403/1−256403/4. (d) Ishii, Y.; Tamura, M.; Kato, R. *J. Phys. Soc. Jpn.* **2007**, *76*, 033704/1−033704/4. (e) Itou, T.; Oyamada, A.; Maegawa, S.; Kubo, K.; Yamamoto, H. M.; Kato, R. *Phys. Rev. B* **2009**, *79*, 174517/1−174517/6.

(8) (a) Itou, T.; Oyamada, A.; Maegawa, S.; Tamura, M.; Kato, R. *Phys. Rev. B* **2008**, *77*, 104413/1−104413/5. (b) Itou, T.; Oyamada, A.; Maegawa, S.; Kato, R. *Nat. Phys.* **2010**, *6*, 673−676. (c) Yamashita, M.; Nakata, N.; Senshu, Y.; Nagata, M.; Yamamoto, H. M.; Kato., R.; Shibauchi, T.; Matsuda, Y. *Science* **2010**, *328*, 1246−1248. (d) Yamashita, S.; Yamamoto, T.; Nakazawa, Y.; Tamura, M.; Kato, R. *Nat. Commun.* **2011**, *2*, 275/1−275/6.

(9) (a) Valade, L.; Legros, J. P.; Bousseau, M.; Cassoux, P.; Garbauskas, M.; Interrante, L. V. *J. Chem. Soc., Dalton Trans.* **1985**, 783−794. (b) Kato, R.; Kobayashi, H.; Kobayashi, A.; Sasaki, Y. *Chem. Lett.* **1985**, 131−134. (c) Kobayashi, H.; Kato, R.; Kobayashi, A.; Sasaki, Y. *Chem. Lett.* **1985**, 191−194. (d) Kim, H.; Kobayashi, A.; Sasaki, Y.; Kato, R.; Kobayashi, H. *Chem. Lett.* **1987**, 1799−1802. (e) Kobayashi, A.; Kato, R.; Kobayashi, H. *Synth. Met.* **1987**, *19*, 635−640. (f) Kato, R.; Kobayashi, H.; Kim, H.; Kobayashi, A.; Sasaki, Y.; Mori, T.; Inokuchi, H. *Synth. Met.* **1988**, *27*, B359−B364. (g) Kato, R.; Kobayashi, H.; Kobayashi, A.; Naito, T.; Tamura, M.; Tajima, H.; Kuroda, H. *Chem. Lett.* **1989**, 1839−1842. (h) Reefman, D.; Cornelissen, J. P.; Haasnoot, J. G.; Degraaff, R. A. G.; Reedijk, J. *Inorg. Chem.* **1990**, *29*, 3933−3935. (i) Miyazaki, A.; Izuoka, A.; Sugawara, T. *Bull. Chem. Soc. Jpn.* **1993**, *66*, 2832−2839. (j) Veldhuizen, Y. S. J.; Veldman, N.; Spek, A. L.; Faulmann, C.; Haasnoot, J. G.; Reedijk, J. *Inorg. Chem.* **1995**, *34*, 140−147. (k) Cornelissen, J. P.; Muller, E.; Vaassens, P. H. S.; Haasnoot, J. G.; Reedijk, J.; Cassoux, P. *Inorg. Chem.* **1992**, *31*, 2241−2248.

(10) Kobayashi, A.; Kim, H.; Sasaki, Y.; Kato, R.; Kobayashi, H.; Moriyama, S.; Nishio, Y.; Kajita, K.; Sasaki, W. *Chem. Lett.* **1987**, *16*, 1819−1822.

(11) Fujiwara, M.; Kato, R. *J. Chem. Soc., Dalton Trans.* **2002**, 3763−3770.

(12) (a) Kosaka, Y.; Yamamoto, H. M.; Nakao, A.; Tamura, M.; Kato, R. *J. Am. Chem. Soc.* **2007**, *129*, 3054−3055. (b) Fujiyama, S.; Shitade, A.; Kanoda, K.; Kosaka, Y.; Yamamoto, H. M.; Kato, R. *Phys. Rev. B* **2008**, *77*, 060403. (c) Hazama, K.; Uji, S.; Takahide, Y.; Kimata, M.; Satsukawa, H.; Harada, A.; Terashima, T.; Kosaka, Y.; Yamamoto, H. M.; Kato, R. *Phys. Rev. B* **2011**, *83*, 165129.

(13) (a) Yamamoto, H. M.; Yamaura, J.; Kato, R. *J. Am. Chem. Soc.* **1998**, *120*, 5905−5913. (b) Yamamoto, H. M.; Maeda, R.; Yamaura, J.; Kato, R. *J. Mater. Chem.* **2001**, *11*, 1034−1041. (c) Yamamoto, H. M.; Kosaka, Y.; Maeda, R.; Yamaura, J.; Nakao, A.; Nakamura, T.; Kato, R. *ACS Nano* **2008**, *2*, 143−155.
(14) Lindqvist, O.; Sjölin, L.; Sieler, J.; Steimecke, G.; Hoyer, E. *Acta Chem. Scand.* **1979**, *33A*, 445−448.
(15) Kushch, N.; Faulmann, C.; Cassoux, P.; Valade, L.; Malfant, I.; Legros, J.-P.; Bowlas, C.; Errami, A.; Kobayashi, A.; Kobayashi, H. *Mol. Cryst. Liq. Cryst.* **1996**, *284*, 247−258.
(16) (a) Clark, T.; Hennemann, M.; Murray, J.; Politzer, P. *J. Mol. Model.* **2007**, *13*, 291−296. (b) Metrangolo, P.; Meyer, F.; Pilati, T.; Resnati, G.; Terraneo, G. *Angew. Chem., Int. Ed.* **2008**, *47*, 6114−6127.
(17) The temperature is lower than that for **1** (20 K). This difference reflects a weaker intralayer magnetic interaction between the anions for **2** than for **1**. This is consistent with the fact that θ-value is smaller for **2** (−1.8 K) than for **1** (−4.9 K).
(18) No differences in the magnetic properties are observed for H // anion layer and H ⊥ anion layer.
(19) Steimecke, G.; Sieler, H. J.; Krimse, R.; Hoyer, E. *Phosphorus, Sulfur* **1979**, *7*, 49−55.
(20) Sheldrick, G. M. *Acta Crystallogr., Sect. A* **2008**, *64*, 112−122.
(21) Otwinowski, Z.; Minor, W. Processing of X-ray Diffraction Data Collected in Oscillation Mode In *Methods in Enzymology*; Academic Press: New York, 1997; Vol. *276*, p 307
(22) Hoffmann, R. *J. Chem. Phys.* **1963**, *39*, 1397−1412.
(23) Mori, T.; Kobayashi, A.; Sasaki, Y.; Kobayashi, H.; Saito, G.; Inokuchi, H. *Bull. Chem. Soc. Jpn.* **1984**, *57*, 627−633.
(24) In **1**, the Br···S halogen bonds are formed at the 2-position in the cation, while it is not formed at the 5-position. In this situation, the crystal structure must be more influenced by the introduction of an I atom at the 5-position than that at the 2-position. The I atom is more polarizable and forms a stronger halogen bond than the Br atom, and therefore brings another halogen bond at the 5-position in **3**, to afford a different crystal structure.
(25) At the high-temperature region ($30 < T < 300$ K), the magnetic properties of the compounds can be explained by the Curie−Weiss law, where the paramagnetic spins are weakly and antiferromagnetically interacting with each other as indicated by the Weiss temperature (−4.9 K for **1** and −1.8 K for **2**). This magnetic situation changes at lower temperature as a result of the evolution of short-range AFM ordering domains, in which the stronger AFM interaction than that observed at high temperature region is dominant between the spins. At 2 K, most of the spins (roughly 83% as deduced from the heat capacity measurements) in the crystal participate in the formation of the short-range AFM domains, and thus the magnetization does not saturate even at 70 kOe.